4

SORET AND DUFOUR EFFECT ON TWO-DIMENSIONAL FLOW OF CASSON FLUID

Content of this chapter is published in:

Materials Today: Proceedings (Elsevier) doi.org/10.1016/j.matpr.2020.11.061.

SORET AND DUFOUR EFFECT ON TWO-DIMENSIONAL FLOW OF CASSON FLUID

In fluid mechanics, fluid flow can be described either by one, two or three-dimensional space coordinates. Generally two or three dimensional fluid flow give better description of physical flow compared to that of one dimensional fluid flow problems. Though, this frequently lead to highly non-linear coupled governing equations and consequently seems to be more difficult to solve. This chapter deals with effects of magnetic field and thermal radiation on two dimensional Casson fluid flow. Important phenomena like chemical reaction, heat generation, heat absorption, Soret effect and Dufour effect are also taken in account.

4.1 Introduction of the problem:

The theoretic and investigational study of viscous incompressible non-Newtonian fluids are extensive. Casson fluid model is a non-Newtonian fluid model with yield stress. Casson fluid model was presented by Casson [102] for pigment-oil suspensions behavior of the flow. Few examples of this type of fluids are honey, tomato sauce, soup, jelly, concentrated fruit juices, etc. Sandeep et al. [106] discussed modified kinematic viscosity model for 3D-Casson fluid flow. Hamid et al. [67 - 68] considered heat transfer effects on Casson fluid flow problems.

The MHD consideration is one of the important parameters by which cooling rate can be controlled and the product of desired quality can be achieved. Magnetohydrodynamics (often referred to as MHD) deals with the dynamics of fluids having non-negligible electrical conductivity which interact with a magnetic field. MHD has several applications, namely, fusion research, MHD accelerator and power generator.

The effect of radiation is much important when there are difference temperatures at the surface and the ambient temperatures. Further, the radiation effects on MHD convective flow problems are more significant in electrical power generation, solar power technology and astrophysical ground. Few representative examinations interconnected with the phenomenon of thermal radiation can be found in the attempts [35, 50, 82, 86, 120]. The transfer of heat and mass together affects each other, and this will cause the cross-diffusion effect. The heat transfer produced by concentration gradient is called the diffusion-thermo or Dufour effect whereas, mass transfer produced by temperature gradient is called Soret or thermal-diffusion effect. Hayat et al. [147,150]

studied soret and heat generation effects on MHD flow with different fluid. Patel [45] and Prasad et al. [157] considered cross diffusion effects on mixed convective MHD flow of Casson fluid through porous medium. Recently, Mittal and Patel [6] defined the solution of thermophoresis and Brownian motion on mixed convection two dimensional MHD Casson fluid flow with non-linear radiation and heat generation.

4.2 Novelty of the chapter:

The main objective of present work to develop mathematical modeling of Soret and Dufour effects on MHD Casson fluid flow in the presence of thermal radiation. The simplified systems of ordinary differential equations are solved using the Homotopy analysis method.

4.3 Mathematical Formulation of the Problem:

Let us consider the steady MHD two dimensional Casson fluid flow over a heated stretched surface at $y = 0$ as shown in Figure 4.1. A Cartesian coordinate system (x, y) are chosen such that x- axis is parallel to stretched surface whereas $y - axis$ as normal to it. A constant magnetic field B_0 is applied in the transverse direction to the surface.

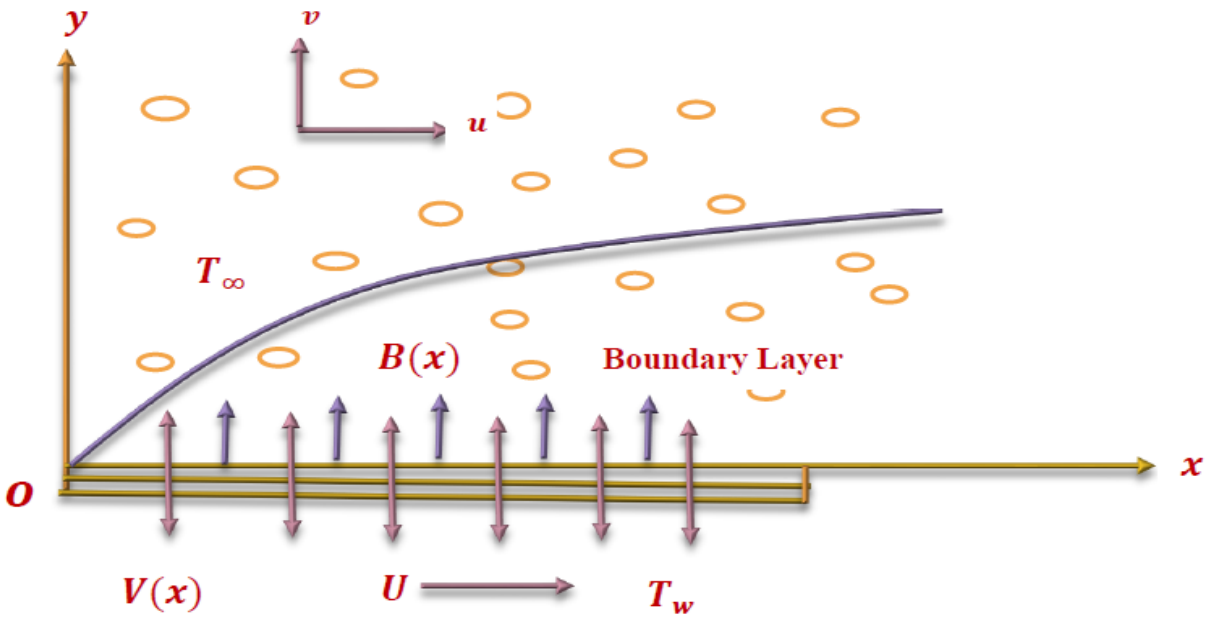

Figure 4.1: Physical sketch of the problem

Due to small magnetic Reynold number induced magnetic field are negligible. Also, fluid is incompressible and flow in two dimensional. We consider this problem due to the effects of soret and dufour effects with chemical reaction and heat generation/absorption on the MHD flow.

The resulting boundary layer equations in MHD flow under consideration are

$$\frac{\partial u}{\partial x}+\frac{\partial v}{\partial y}=0 \tag{4.1}$$

$$\left(u\frac{\partial u}{\partial x}+v\frac{\partial u}{\partial y}\right)=\left(1+\frac{1}{\gamma}\right)\frac{\partial^2 u}{\partial y^2}-\frac{\sigma B_0^2}{\rho}u+g\beta_T(T-T_\infty)+g\beta_C(C-C_\infty) \tag{4.2}$$

$$\left(u\frac{\partial T}{\partial x}+v\frac{\partial T}{\partial y}\right)=\frac{k}{\rho c_p}\frac{\partial^2 T}{\partial y^2}-\frac{1}{\rho c_p}\frac{\partial q_r}{\partial y}+\frac{Q_0}{\rho c_p}(T-T_\infty)+\frac{D_M k_T}{C_s C_p}\frac{\partial^2 C}{\partial y^2} \tag{4.3}$$

$$\left(u\frac{\partial C}{\partial x}+v\frac{\partial C}{\partial y}\right)=D_M\frac{\partial^2 C}{\partial y^2}-k_2'\,(C'-C'_\infty)+\frac{D_M k_T}{T_m}\frac{\partial^2 T}{\partial y^2} \tag{4.4}$$

$$u=ax;\ v=0;\ T=T_w;C=C_w\ at\ y=0 \tag{4.5}$$

$$u\to 0, T\to T_\infty,\ C\to C_\infty;\ as\ y\to\infty\ and\ t\geq 0 \tag{4.6}$$

$$\eta=y\sqrt{\frac{a}{\nu}},\ u=axf'(\eta), v=-\sqrt{a\nu}f(\eta),\ \theta(\eta)=\frac{T-T_\infty}{T_w-T_\infty}, C(\eta)=\frac{(C'-C'_\infty)}{(C'_w-C'_\infty)} \tag{4.7}$$

The local radiant for the case of an optically thin gray gas is expressed by Rosseland approximation [127].

$$\frac{\partial q_r}{\partial y}=-4a^*\sigma^*(T'^4_\infty-T'^4)$$

Using the Taylor's series, expand T'^4 about T'_∞ and neglecting higher order terms,

$$T'^4\cong 4T'^3_\infty T'-3T'^4_\infty$$

Therefore, the governing momentum, energy and mass equations for this problem are given in dimensionless form by:

$$\left(1+\frac{1}{\gamma}\right)f'''+\frac{3}{4}ff''-\frac{1}{2}f'^2+Gr\theta+Gm\,C-M^2f'=0 \tag{4.8}$$

$$\left(\frac{1+\frac{4}{3}R}{Pr}\right)\theta''+f\theta'-\theta f'+H\theta+Df\,C''=0 \tag{4.9}$$

$$\frac{1}{Sc}C''+fC'-Kr\,C+Sr\theta''=0 \tag{4.10}$$

$$f(0)=0, f'(0)=1\,, f'(\infty)=0\,,$$
$$\theta(0)=1, \theta(\infty)=0\,,$$
$$C(0)=1, C(\infty)=0\,, \tag{4.11}$$

where

$$M^2 = \frac{\sigma {B_0}^2}{\rho {U_0}^2} t_0,\ \gamma = \frac{\mu_B \sqrt{2\pi_c}}{P_y},\ Sc = \frac{\nu}{D_M},\ R = -\frac{16\, a^* \sigma^* v^2 {T'}_\infty^{\,3}}{k_4 {U_0}^2},\ Pr = \frac{\rho c_p}{k}, Df = \frac{D_M k_T}{C_s C_p} \frac{C_w - C_\infty}{(T_w - T_\infty)\vartheta},$$

$$Sr = \frac{D_M k_T}{T_m \vartheta} \frac{T_w - T_\infty}{(C_w - C_\infty)}, Gr = \frac{v g \beta_T (T - T_\infty)}{U_0^3}, Gm = \frac{v g \beta_C (C - C_\infty)}{U_0^3}, H = \frac{Q_0 v^2}{k\, U_0^2}, Kr = \frac{k_2}{\vartheta^2} \quad (4.12)$$

Dimensionless expression of the local skin-friction coefficient, the local Nusselt number and the local Sherwood number are

$$Re^{1/2} C_f = \left(1 + {}^1/_\gamma\right) f''(0), \quad (4.13)$$

$$Nu(Re)^{-1/2} = -\theta'(0), \quad (4.14)$$

$$Sh(Re)^{-1/2} = -\mathrm{C}'(0). \quad (4.15)$$

4.4 Solution by Homotopy Analysis Method:

Equations (4.08) – (4.10) are coupled non-linear ordinary differential equations and exact solutions are not possible. To solve these equations together with the boundary conditions (4.11), the modified homotopy analysis method (HAM) suggested by Liao [122] is employed.

Initial guess is given by:

$$f_0(\eta) = 1 - e^{-\eta};\ \theta_0(\eta) = e^{-\eta};\ C_0(\eta) = e^{-\eta}; \quad (4.16)$$

with auxiliary linear operators:

$$L_f = \frac{\partial^3 f}{\partial \eta^3} - \frac{\partial f}{\partial \eta}\ ,\ L_\theta = \frac{\partial^2 \theta}{\partial \eta^2} + \theta\ ,\ L_{\mathrm{C}} = \frac{\partial^2 \mathrm{C}}{\partial \eta^2} - \mathrm{C} \quad (4.17)$$

Satisfying

$$L_f(B_1 + B_2 e^{\eta} + B_3 e^{-\eta}) = 0,\ L_\theta(B_4 \cos\eta + B_5 \sin\eta) = 0,\quad L_{\mathrm{C}}(B_6 e^{\eta} + B_7 e^{-\eta}) = 0. \quad (4.18)$$

where $B_1,\ B_2, \ldots, B_7$ are the arbitrary constants.

The zeroth order deformation problems are constructed as follows:

$$(1-p) L_f\left[\hat{f}(\eta;\ p) - f_0(\eta)\right] = p \hbar_f N_f\left[\hat{f}(\eta;\ p), \hat{\theta}(\eta;\ p), \hat{\mathrm{C}}(\eta;\ p)\right], \quad (4.19)$$

$$(1-p) L_\theta\left[\hat{\theta}(\eta;\ p) - \theta_0(\eta)\right] = p \hbar_\theta N_\theta\left[\hat{f}(\eta;\ p), \hat{\theta}(\eta;\ p), \hat{\mathrm{C}}(\eta;\ p)\right], \quad (4.20)$$

$$(1-p) L_{\mathrm{C}}\left[\hat{\mathrm{C}}(\eta;\ p) - \mathrm{C}_0(\eta)\right] = p \hbar_{\mathrm{C}} N_{\mathrm{C}}\left[\hat{f}(\eta;\ p), \hat{\theta}(\eta;\ p), \hat{\mathrm{C}}(\eta;\ p)\right], \quad (4.21)$$

Subject to the boundary conditions:

$\hat{f}(0;\ p) = 0, \quad \hat{f}'(0;\ p) = 1;$ (4.22)

$\hat{f}'(\infty;\ p) = 0;$ (4.23)

$\hat{\theta}(0;\ p) = 1, \quad \hat{\theta}(\infty;\ p) = 0;$ (4.24)

$\hat{\mathrm{C}}(0;\ p) = 1, \quad \hat{\mathrm{C}}(\infty;\ p) = 0.$ (4.25)

The nonlinear operator are defined as

$$N_f\left[\hat{f}(\eta;\ p), \hat{\theta}(\eta;\ p), \hat{\mathrm{C}}(\eta;\ p)\right] = \left(1 + \frac{1}{\gamma}\right)\frac{\partial^3 \hat{f}}{\partial \eta^3} + \frac{3}{4}\hat{f}\frac{\partial^2 \hat{f}}{\partial \eta^2} - \frac{1}{2}\left(\frac{\partial \hat{f}}{\partial \eta}\right)^2 + Gr\hat{\theta} + Gm\hat{\mathrm{C}} - \left(M^2 + \frac{1}{k}\right)\frac{\partial \hat{f}}{\partial \eta}, \quad (4.26)$$

$$N_\theta\left[\hat{f}(\eta;\ p), \hat{\theta}(\eta;\ p), \hat{\mathrm{C}}(\eta;\ p)\right] = \left(\frac{1+\frac{4}{3}Nr}{Pr}\right)\frac{\partial^2 \hat{\theta}}{\partial \eta^2} + \hat{f}\frac{\partial \hat{\theta}}{\partial \eta} - \hat{\theta}\frac{\partial \hat{f}}{\partial \eta} + H\hat{\theta} + D_f\frac{\partial^2 \hat{\mathrm{C}}}{\partial \eta^2}, \quad (4.27)$$

$$N_{\mathrm{C}}\left[\hat{f}(\eta;\ p), \hat{\theta}(\eta;\ p), \hat{\mathrm{C}}(\eta;\ p)\right] = \frac{1}{Sc}\frac{\partial^2 \hat{\mathrm{C}}}{\partial \eta^2} + \hat{f}\frac{\partial \hat{\mathrm{C}}}{\partial \eta} - Kr\hat{\mathrm{C}} + Sr\frac{\partial^2 \hat{\theta}}{\partial \eta^2} \quad (4.28)$$

Where $\hat{f}(\eta;\ p), \hat{\theta}(\eta;\ p)$ and $\hat{\mathrm{C}}(\eta;\ p)$ are unknown functions with respect to η and p. $\hbar_f$, $\hbar_\theta$ and $\hbar_{\mathrm{C}}$ are the non-zero auxiliary parameters and N_f, N_θ and N_{C} are the nonlinear operators.

Also $p \in (0,\ 1)$ is an embedding parameter. For $p = 0$ and $p = 1$ we have

$\hat{f}(\eta; 0) = f_0(\eta), \hat{f}(\eta; 1) = f(\eta),$ (4.27)

$\hat{\theta}(\eta; 0) = \theta_0(\eta), \hat{\theta}(\eta; 1) = \theta(\eta),$ (4.28)

$\hat{\mathrm{C}}(\eta; 0) = \mathrm{C}_0(\eta), \hat{\mathrm{C}}(\eta; 1) = \mathrm{C}(\eta),$ (4.29)

In other words, when variation of p is taken from 0 to 1 then $\hat{f}(\eta;\ p)$, $\hat{\theta}(\eta;\ p)$ and $\hat{\mathrm{C}}(\eta;\ p)$ vary from $f_0(\eta), \theta_0(\eta)$, and $\mathrm{C}_0(\eta)$ to $f(\eta), \theta(\eta)$, and $\mathrm{C}(\eta)$. Taylor's series expansion of these functions yields the following:

$\hat{f}(\eta;\ p) = f_0(\eta) + \sum_{m=1}^{\infty} f_m(\eta)p^m,$ (4.30)

$\hat{\theta}(\eta;\ p) = \theta_0(\eta) + \sum_{m=1}^{\infty} \theta_m(\eta)p^m,$ (4.31)

$\hat{\mathrm{C}}(\eta;\ p) = \mathrm{C}_0(\eta) + \sum_{m=1}^{\infty} \mathrm{C}_m(\eta)p^m,$ (4.32)

Where

$$f_m(\eta) = \frac{1}{m!}\left[\frac{\partial^m f(\eta; p)}{\partial p^m}\right]_{p=0}, \quad (4.33)$$

$$\theta_m(\eta) = \frac{1}{m!}\left[\frac{\partial^m \theta(\eta; p)}{\partial p^m}\right]_{p=0}, \quad (4.34)$$

$$\mathrm{C}_m(\eta) = \frac{1}{m!}\left[\frac{\partial^m \mathrm{C}(\eta; p)}{\partial p^m}\right]_{p=0}, \tag{4.35}$$

It should be noted that the convergence in the above series strongly depends upon $\hbar_f, \hbar_\theta$ and $\hbar_{\mathrm{C}}$. Assuming that these nonzero auxiliary parameters are chosen so that Equations (4.30)–(4.32) converges at $p = 1$, Hence one can obtain the following:

$$f(\eta) = f_0(\eta) + \sum_{m=1}^{\infty} f_m(\eta), \tag{4.36}$$

$$\theta(\eta) = \theta_0(\eta) + \sum_{m=1}^{\infty} \theta_m(\eta), \tag{4.37}$$

$$\mathrm{C}(\eta) = \mathrm{C}_0(\eta) + \sum_{m=1}^{\infty} \mathrm{C}_m(\eta), \tag{4.38}$$

Differentiating the zeroth order deformation (4.19) – (4.21) and (4.22) – (4.25) m times with respect to p and substituting $p = 0$, and finally dividing by ! , we obtain the m^{th} order deformation ($m \geq 1$).

$$L_f[f_m(\eta) - \chi_m f_{m-1}(\eta)] = \hbar_f R_{f,m}(\eta), \tag{4.39}$$

$$L_\theta[\theta_m(\eta) - \chi_m \theta_{m-1}(\eta)] = \hbar_\theta R_{\theta,m}(\eta), \tag{4.40}$$

$$L_{\mathrm{C}}[\mathrm{C}_m(\eta) - \chi_m \mathrm{C}_{m-1}(\eta)] = \hbar_{\mathrm{C}} R_{\mathrm{C},m}(\eta), \tag{4.41}$$

Subject to the boundary conditions

$$f_m(0) = 0, \tag{4.42}$$

$$f_m'(0) = f_m'(\infty) = 0, \tag{4.43}$$

$$\theta_m(0) = \theta_m(\infty) = 0, \tag{4.44}$$

$$\mathrm{C}_m(0) = \mathrm{C}_m(\infty) = 0, \tag{4.45}$$

with

$$R_{f,m}(\eta) = \left(1 + \frac{1}{\gamma}\right) f_{m-1}''' + \frac{3}{4}\sum_{j=0}^{m-1} f_j f_{m-1-j}'' - \frac{1}{2}\sum_{j=0}^{m-1} f_j'^2 + Gr\theta_{m-1} + Gm\mathrm{C}_{m-1} - \left(M^2 + \frac{1}{k}\right) f_{m-1}' \tag{4.46}$$

$$R_{\theta,m}(\eta) = \left(\frac{1+\frac{4}{3}Nr}{Pr}\right)\theta_{m-1}'' + \sum_{j=0}^{m-1} f_j \theta_{m-1-j}' - \sum_{j=0}^{m-1} f_j' \theta_{m-1-j} + H\theta_{m-1} + D_f \mathrm{C}_{m-1}'' \tag{4.47}$$

$$R_{\mathrm{C},m}(\eta) = \frac{1}{Sc} C_{m-1}'' + \sum_{j=0}^{m-1} f_j \mathrm{C}_{m-1-j}' - Kr\mathrm{C}_{m-1} + Sr\theta_{m-1}'' \tag{4.48}$$

$$\text{with } \chi_m = \begin{cases} 0, & m \leq 1 \\ 1, & m \geq 1 \end{cases}, \tag{4.49}$$

Solving the corresponding m^{th}-order deformation equations,

$$f_m(\eta) = f_m^*(\eta) + B_1 + B_2 e^{\eta} + B_3 e^{-\eta} \tag{4.50}$$

$$\theta_m(\eta) = \theta_m^*(\eta) + B_4 \cos\eta + B_5 \sin\eta \quad (4.51)$$

$$\mathrm{C}_m(\eta) = \mathrm{C}_m^*(\eta) + B_6 e^{\eta} + B_7 e^{-\eta} \quad (4.52)$$

Here $f_m^*, \theta_m^* \; and \; \mathrm{C}_m^*$ are given by are particular solutions of the corresponding m^{th}-order equations and the constants $B_i (\, i = 1,2, \ldots ,7)$ are to be determined by the boundary conditions.

4.4.1 Convergence Analysis

$\hbar$-curves of the functions $\mathrm{f}''(0)$, $\theta'(0)$ and $\mathrm{C}'(0)$ are displayed in Figures 4.2, 4.3 and 4.4. The range for the admissible values of $\hbar_f$, $\hbar_\theta$ and $\hbar_C$ which are $-0.65 \leqslant \hbar_f \leqslant -0.2$, $-0.4 \leqslant \hbar_\theta \leqslant 0.4$ and $-0.8 \leqslant \hbar_C \leqslant -0.4$. From the figures we can observed that solution converge in the range of -0.4 to -0.2.

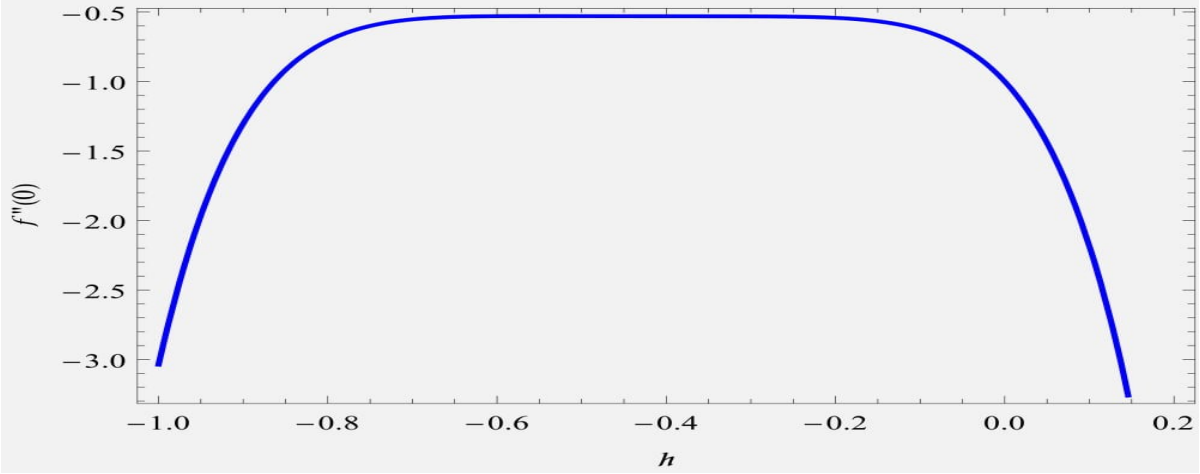

Figure 4.2: h curve for $f''(0)$

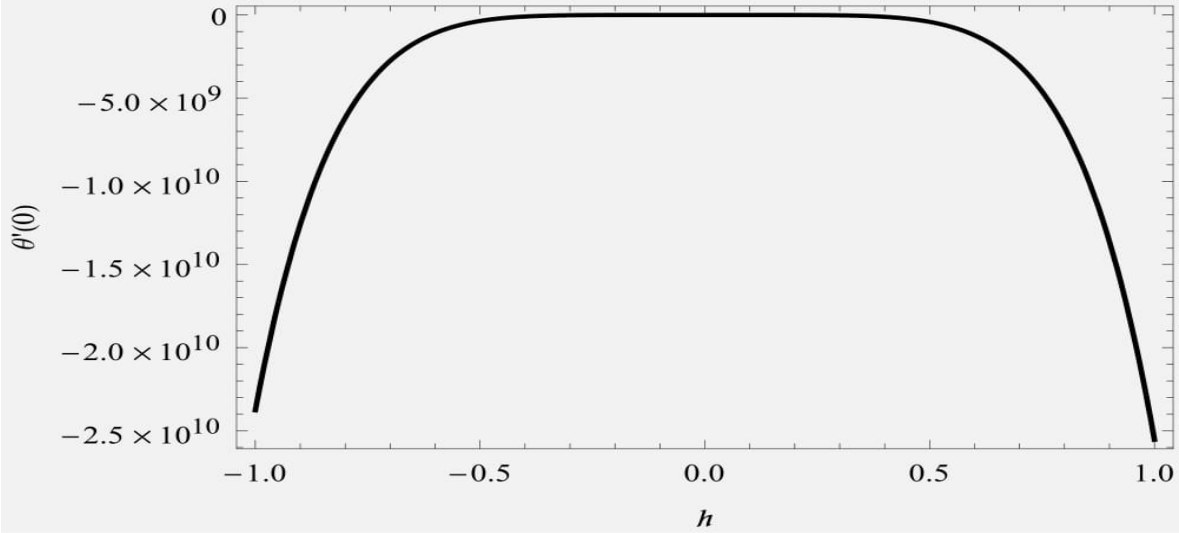

Figure 4.3: h curve for $\theta'(0)$

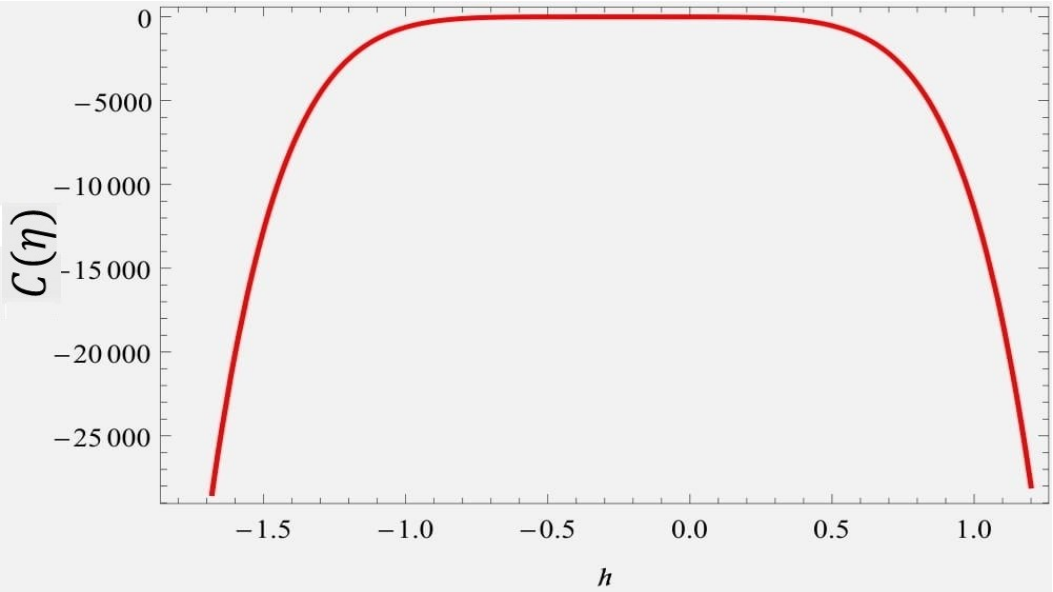

Figure 4.4: h curve for $C'(0)$

4.5 Results and Discussion:

To understand the results of the problem, the solutions are derived using Mathematica. The solution contains long series expressions, which are difficult to show in the manuscript. Obtained results are explained with the help of graphs. Parametric study is performed for Soret number Sr, Dufour number D_f, Radiation parameter R, Magnetic field parameter M and Casson parameter γ. Figure 4.5 show effects of magnetic field M on velocity profiles. It is seen that, velocity in y-direction is decrease with increase in M. Physically, when magnetic parameter M increase the velocity boundary layer thickness decrease. The values of M increase, so as the retarding force, so as a result of that the velocity and velocity boundary layer thickness decrease. Figure 4.6 shows the effect on velocity profiles for different values of Casson parameter γ. It is observed that velocity of the fluid decreases with increasing values Casson parameter γ. An increase in Casson parameter makes nature of the momentum boundary layer thickness shorter and hence motion of the fluid is decelerated. Figure 4.7 show effects of Grashof number Gr on the velocity profile. Grashof number is ratio between the buoyancy forces and viscous forces in fluids. Buoyancy forces drives natural convection as the hot fluid goes up and the cold goes down, and the viscous force tries to stop it. So the increase in Grashof number increases velocity of the fluid.

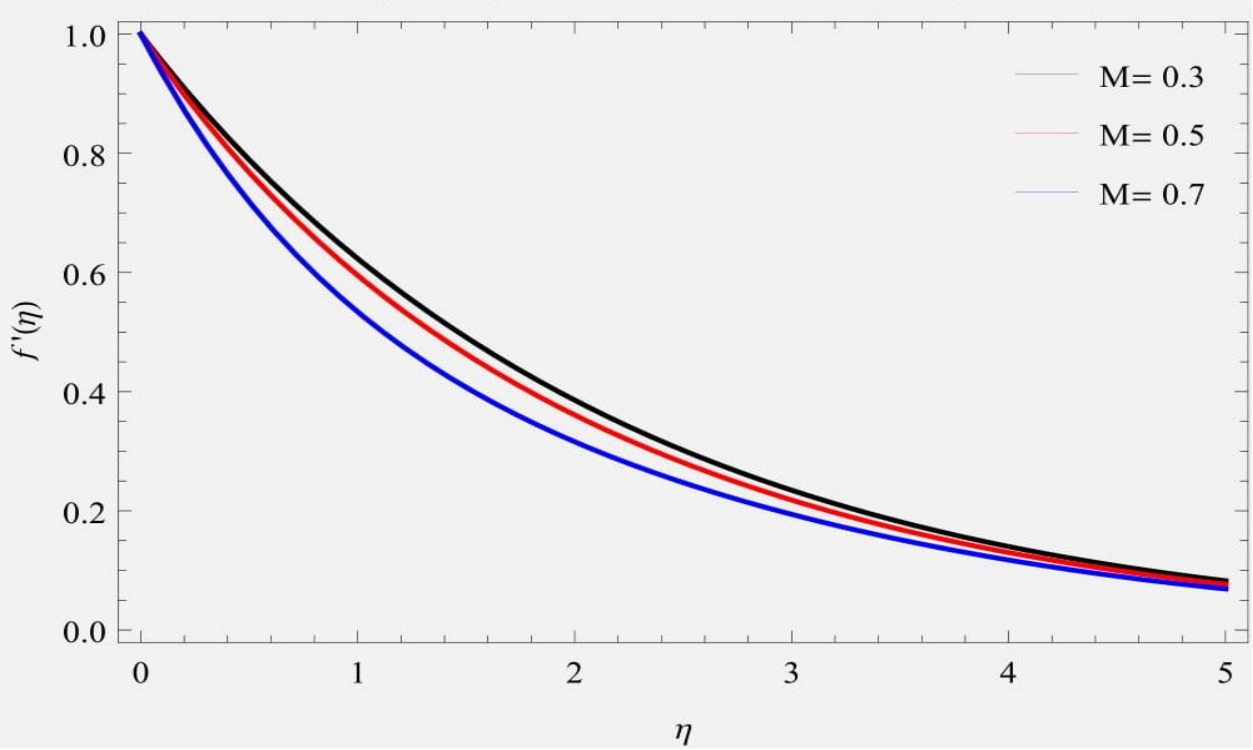

Figure 4.5: Velocity Profile for Different value of M at $k = 0.5, Gr = 1, \gamma = 0.7,$ $Pr = 0.71, Sr = 3, Df = 1, Sc = 0.22, R = 0.2, Kr = 0.2$ *and* $H = 0.1$.

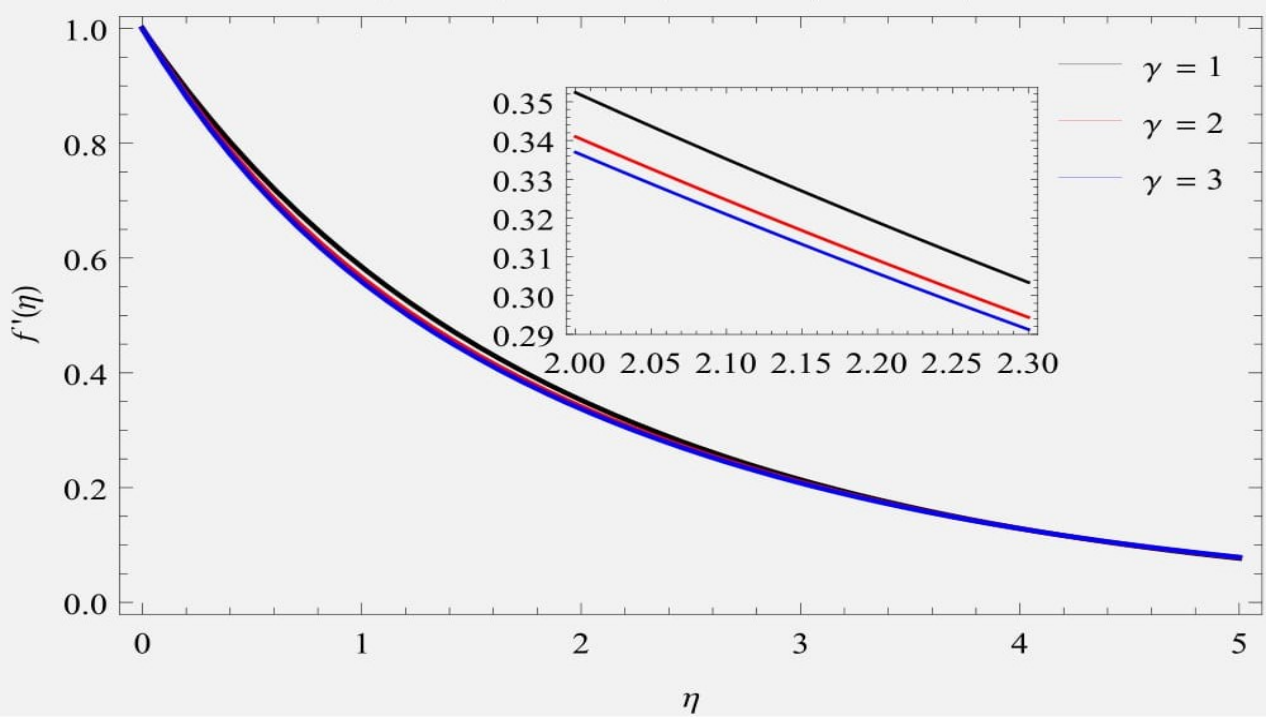

Figure 4.6: Velocity Profile for Different value of $\boldsymbol{\gamma}$ at at $M = 0.5, k = 0.5, Gr = 1, Gm = 1,$ $Pr = 0.71, Sr = 3, Df = 1, Sc = 0.22, R = 0.2, Kr = 0.2$ *and* $H = 0.1$.

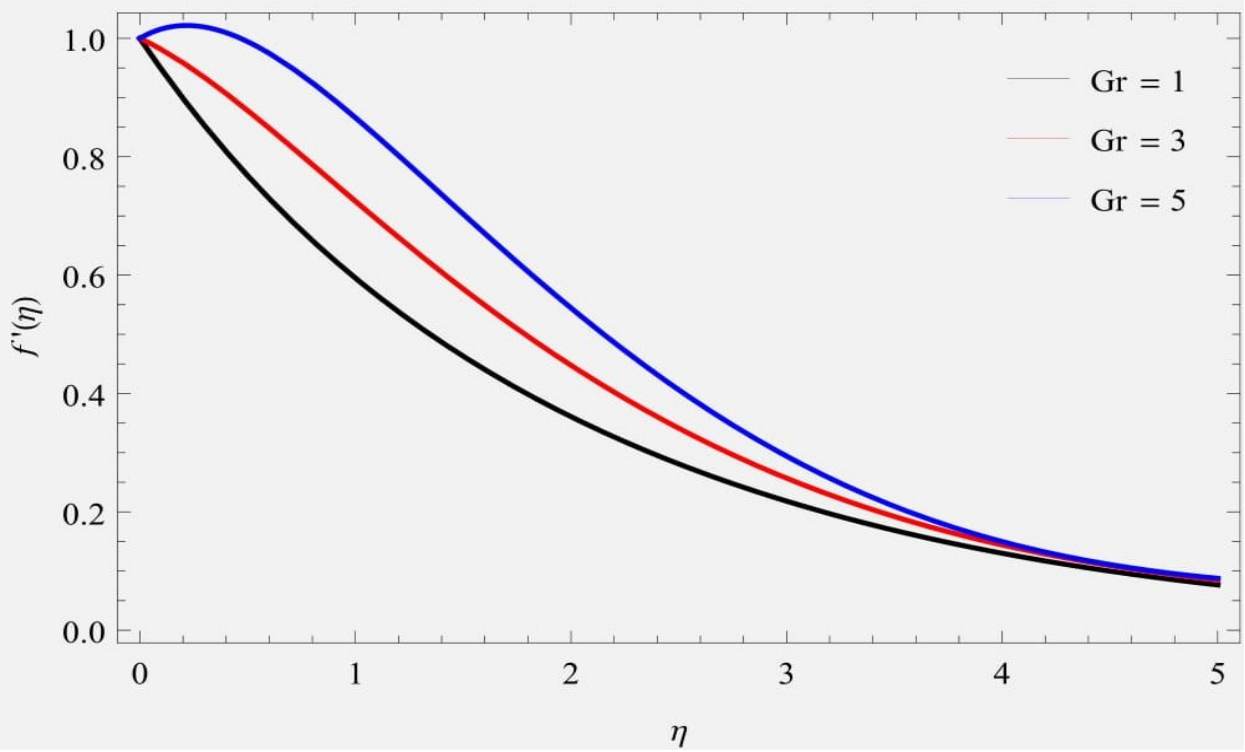

Figure 4.7: Velocity Profile for Different value of Gr at at $M = 0.5, k = 0.5, \gamma = 0.7, Gm = 1, Pr = 0.71, Sr = 3, Df = 1, Sc = 0.22, R = 0.2, Kr = 0.2$ *and* $H = 0.1$.

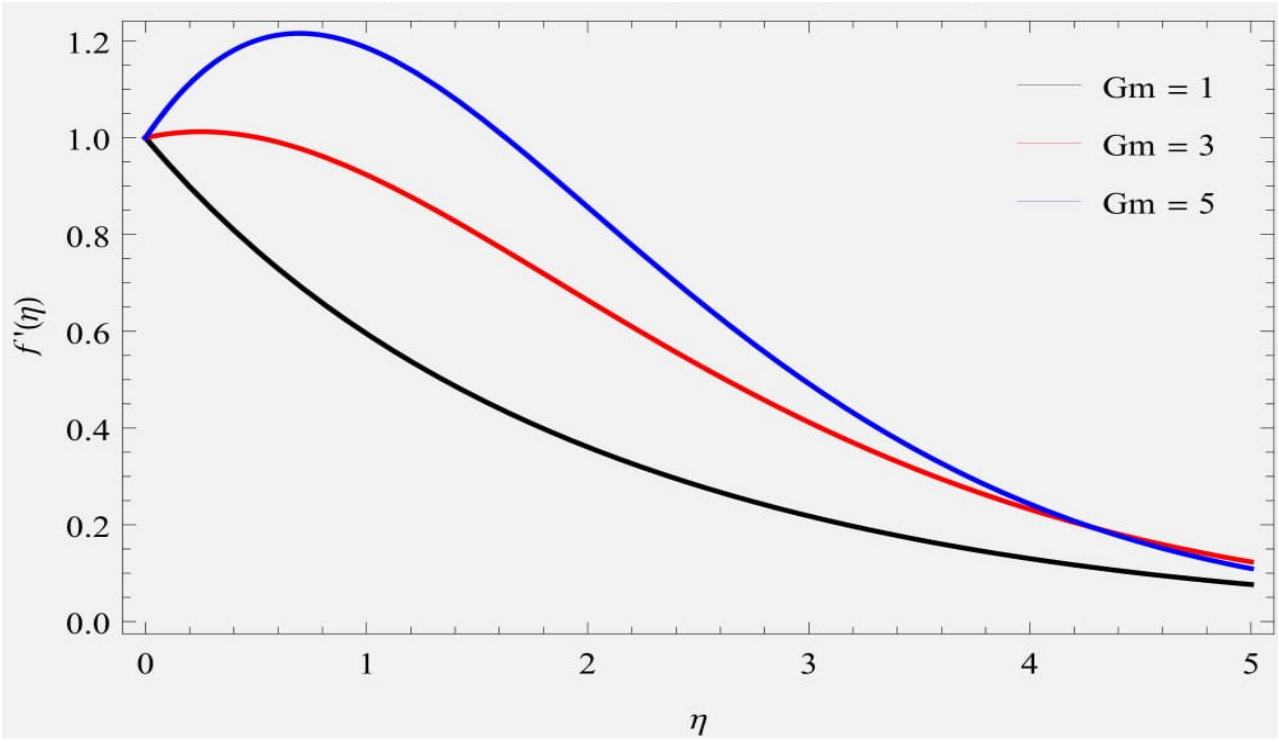

Figure 4.8: Velocity Profile for Different value of Gm at $M = 0.5, k = 0.5, \gamma = 0.7, Gr = 1, Pr = 0.71, Sr = 3, Df = 1, Sc = 0.22, R = 0.2, Kr = 0.2$ *and* $H = 0.1$

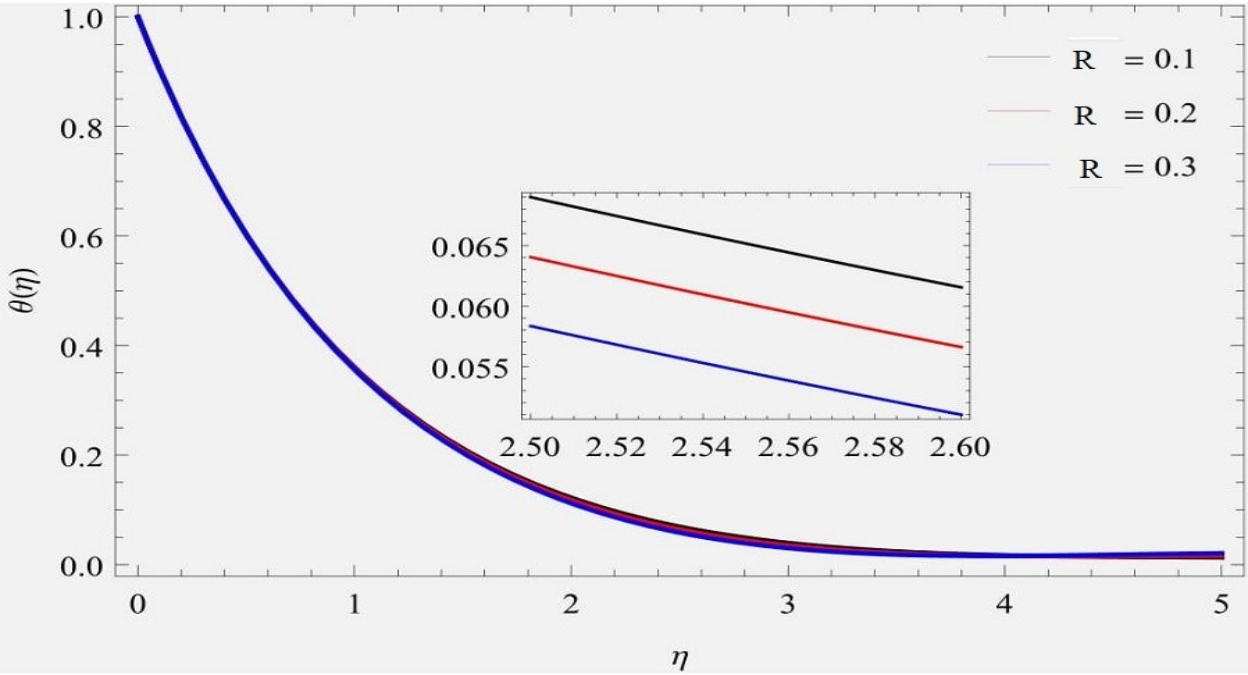

Figure 4.9: Temperature Profile for values of R at $M = 0.5, k = 0.5, \gamma = 0.7, Gr = 1,$ $Gm = 1, Pr = 0.71, Sr = 3, Df = 1, Sc = 0.22, Kr = 0.2$ and $H = 0.1.$

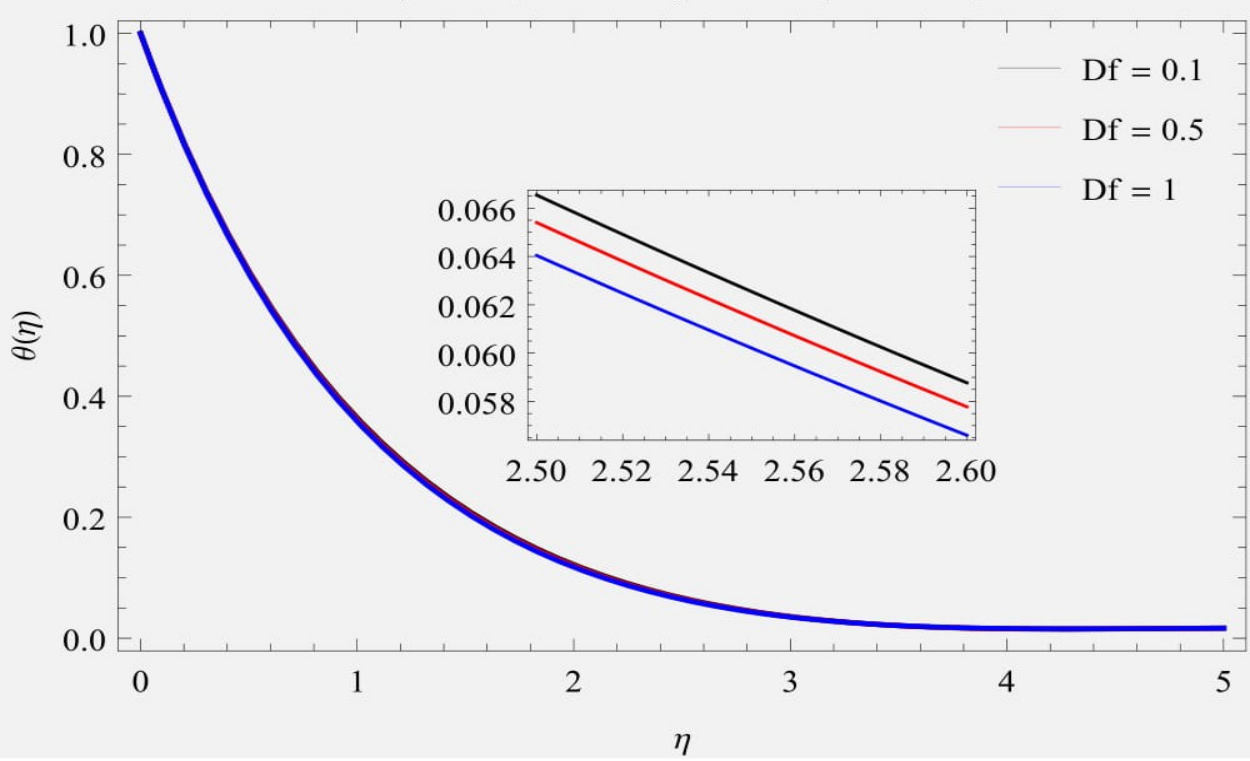

Figure 4.10: Temperature Profile for values of Df at $M = 0.5, k = 0.5, \gamma = 0.7, Gr = 1,$ $Gm = 1, Pr = 0.71, Sr = 3, R = 0.2, Sc = 0.22, Kr = 0.2$ and $H = 0.1.$

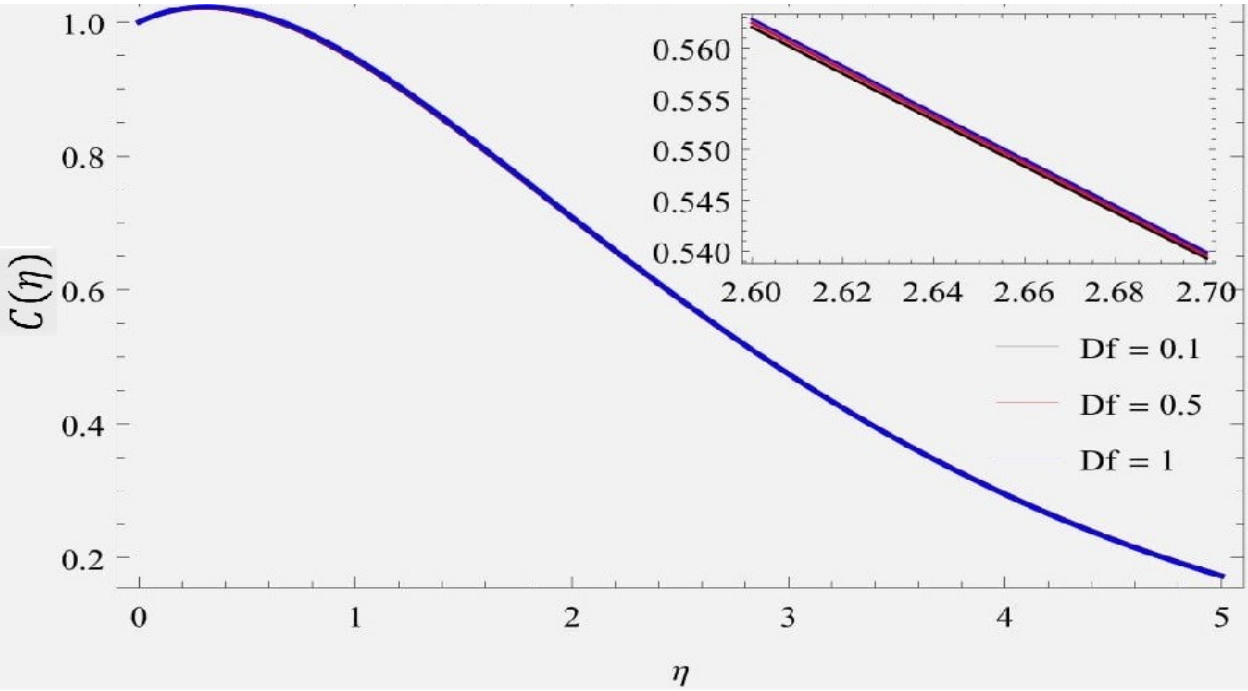

Figure 4.11: Concentration Profile for values of Df at $M = 0.5, k = 0.5, \gamma = 0.7, Gr = 1,$ $Gm = 1, Pr = 0.71, Sr = 3, R = 0.2, Sc = 0.22, Kr = 0.2$ and $H = 0.1.$

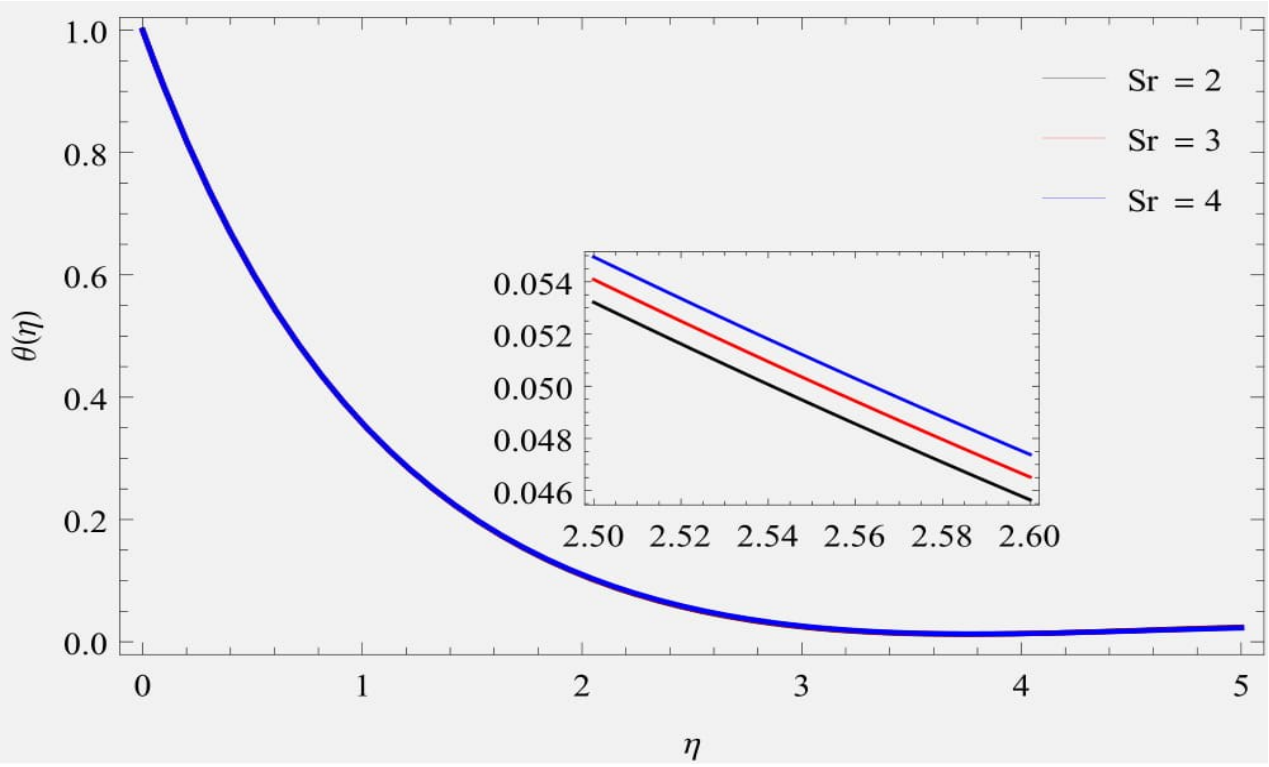

Figure 4.12: Temperature Profile for values of Sr at $M = 0.5, k = 0.5, \gamma = 0.7, Gr = 1,$ $Gm = 1, Pr = 0.71, Df = 1, R = 0.2, Sc = 0.22, Kr = 0.2$ and $H = 0.1.$

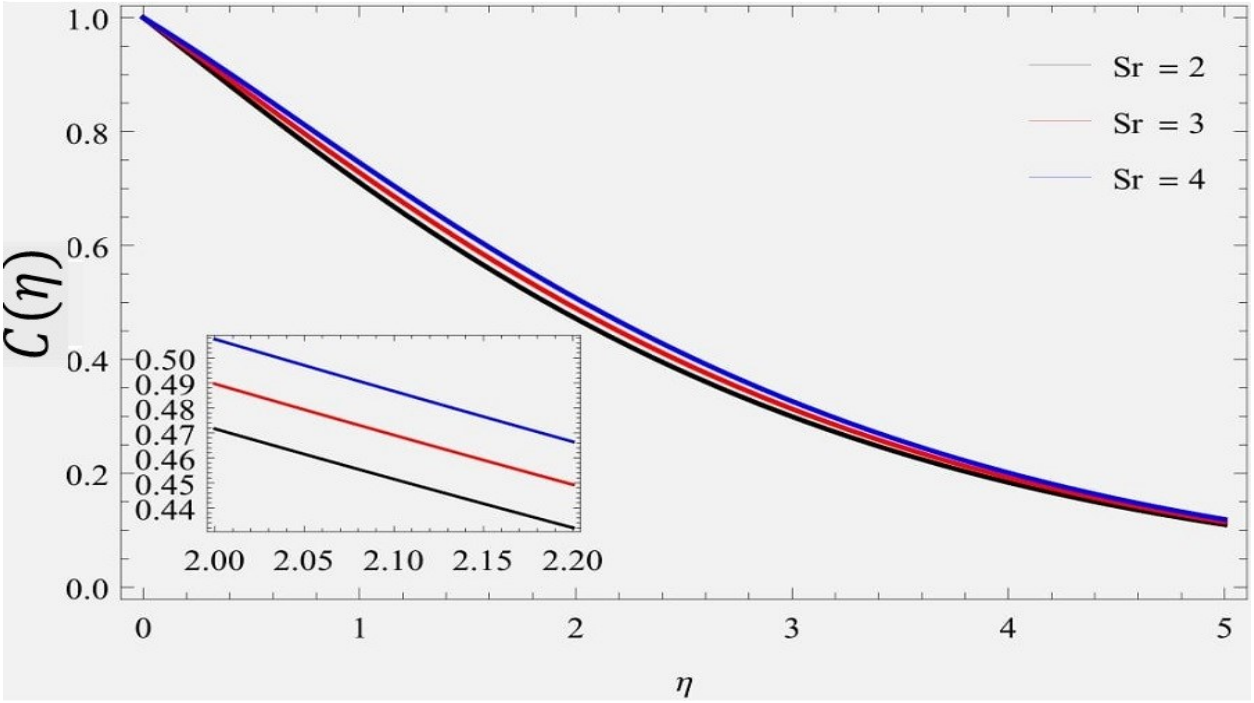

Figure 4.13: Concentration Profile for values of Sr at $M = 0.5, k = 0.5, \gamma = 0.7, Gr = 1, Gm = 1, Pr = 0.71, Df = 1, R = 0.2, Sc = 0.22, Kr = 0.2$ *and* $H = 0.1$.

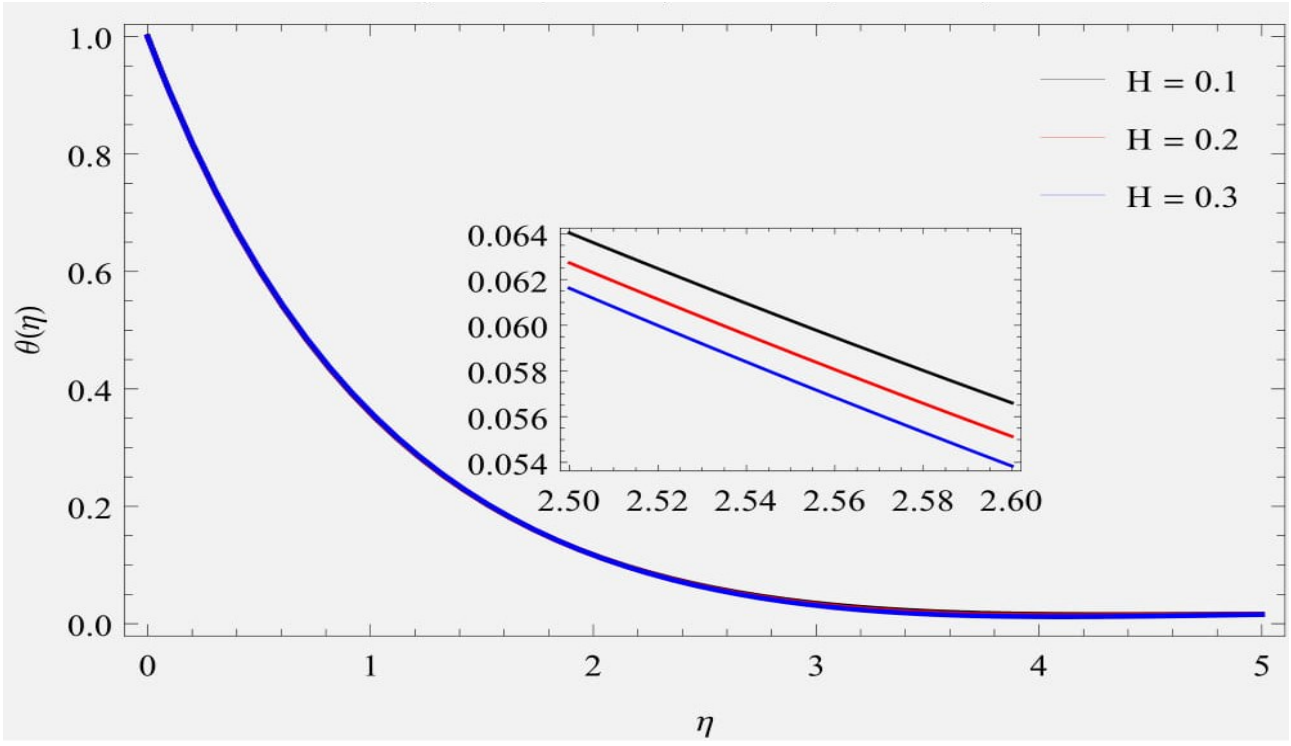

Figure 4.14: Temperature Profile for values of H at $M = 0.5, k = 0.5, \gamma = 0.7, Gr = 1, Gm = 1, Pr = 0.71, Sr = 3, Df = 1, R = 0.2, Sc = 0.22$ *and* $Kr = 0.2$.

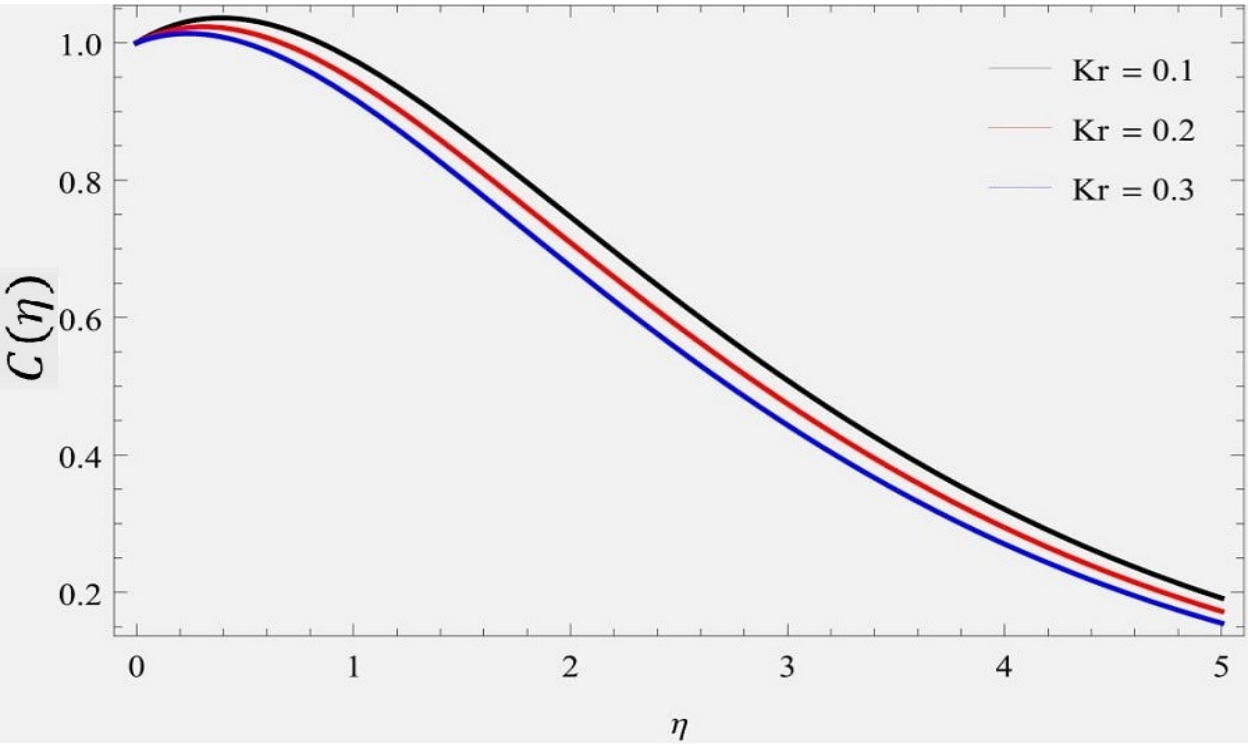

Figure 4.15: Concentration Profile for values of Sr at $M = 0.5, k = 0.5, \gamma = 0.7, Gr = 1,$ $Gm = 1, Pr = 0.71, Sr = 3, Df = 1, R = 0.2, Sc = 0.22$ and $H = 0.1$

Figure 4.8 show effects of mass Grashof number Gm on the velocity profile. The Grashof number Gm expresses the ratio of the species buoyancy force to the viscous hydrodynamic force. The fluid velocity increases and the peak value is more distinguishing due to increase in the species buoyancy force. Figure 4.9 show effects of thermal radiation parameter R on temperature profiles. It shows that increase in thermal radiation parameter R decrease in heat transfer process. Figures 4.10-4.13 show effects of soret and dufour effect on temperature and concentration profiles. It is seen that soret number tends to improve heat transfer process and as well as mass transfer process, while dufour number tend to reduced heat transfer and improved in mass transfer. Figure 4.14 exhibits the temperature profiles for different values of heat generation H. It is observed that heat transfer process decreases with increase in H. Figure 4.15 exhibits the concentration profiles for different values of chemical reaction Kr. It is seen that concentration profile decreases with increase in Kr. The fluid motion is retarded on the account of chemical reaction. This shows that the destructive reaction $Kr > 0$ leads to fall in the concentration field.

Table 4.1: Skin friction variation at $Pr = 0.71$ and $Sc = 0.22$

M	k	γ	Gr	Gm	Sr	Df	R	Kr	H	$\left(1+{}^{1}/_{\gamma}\right)f''(0)$
0.5	0.5	0.7	1	1	3	1	0.2	0.2	0.1	-1.3135047612
0.6										-1.3793674813
0.7										-1.4544062817
	0.6									-1.1028571679
	0.7									-0.9421058268
		0.8								-1.2247410297
		0.9								-1.1679848046
			2							-0.8700017377
			3							-0.4127253077
				2						-0.5106438326
				3						0.2451789807
					3.1					-1.3072264525
					3.2					-1.3009419557
						1.1				-1.3127685040
						1.2				-1.3119483186
							0.3			-1.3116228569
							0.4			-1.3085540338
								0.3		-1.3316732161
								0.4		-1.3486584024
									0.2	-1.3142521275
									0.3	-1.3147865412

Table 4.1 shows the effects of various parameters on skin friction coefficient. By enhancing the values of M and Kr, skin friction coefficient decreasing while it appreciate for the other parameter of the system.

Table 4.2: Nusselt Number variation at $Pr = 0.71$ and $Sc = 0.22$

M	k	γ	Gr	Gm	Sr	Df	R	Kr	H	$-\theta'(0)$
0.5	0.5	0.7	1	1	3	1	0.2	0.2	0.1	1.0044571948
0.6										1.0043515974
0.7										1.0042208708
	0.6									1.0047713778
	0.7									1.0050057098
		0.8								1.0043162214
		0.9								1.0042342225
			2							1.0052474834
			3							1.0058756312
				2						1.0056568002
				3						1.0067259193
					3.1					1.0048203076
					3.2					1.0051901551
						1.1				1.0058243831
						1.2				1.0071945120
							0.3			1.0042501278
							0.4			1.0055640727
								0.3		1.0038934627
								0.4		1.0033415795
									0.2	1.0015461342
									0.3	0.9983075581

Table 4. 2 shows the effects of various parameters on Nusselt number. By increasing the values of M,γ, Kr and H, Nusselt number decreasing while it increasing for the other parameter of the system.

Table 4.3: Sherwood Number variation at $Pr = 0.71$ and $Sc = 0.22$

M	k	γ	Gr	Gm	Sr	Df	R	Kr	H	$-C'(0)$
0.5	0.5	0.7	1	1	3	1	0.2	0.2	0.1	−0.1567652715
0.6										−0.1583796705
0.7										−0.1602161964
	0.6									−0.1514492779
	0.7									−0.1471772703
		0.8								−0.1579623639
		0.9								−0.1588375632
			2							−0.1479023517
			3							−0.1393181389
				2						−0.1336831022
				3						−0.1119284635
					3.1					−0.1737726272
					3.2					−0.1907924952
						1.1				−0.1573316973
						1.2				−0.1578655138
							0.3			−0.1553020862
							0.4			−0.1539433240
								0.3		−0.1179351853
								0.4		−0.0811038847
									0.2	−0.1550745277
									0.3	−0.1531771595

Table 4.3 shows the effects on Sherwood number. By increasing the values of M, γ and Sc, Sherwood number decreasing while it increasing for the remaining parameter of the system.

4.6 Conclusion:

The objective of this research is to obtain semi–analytic solution for two dimensional Casson fluid flow and observe radiation, heat generation or absorption and chemical reaction effects.

Key remarks for the conclusions can be summarized as follows.

- Velocity profile declines with escalation in Magnetic parameter and Casson parameter γ
- Velocity profile increase with increase in Grashof Numbers $Gr, Gm.$
- Temperature increases with increase in Soret effect Sr.
- Temperature tends to decrease with rising radiation parameter R, Dufour effect Df and Heat generation parameter H.
- Concentration profile increase with increase in Soret effect Sr and Dufour effect Df and decrease with increase in chemical reaction Kr.